Advanced Numerical Modeling of the Dispersion of Ceramic Nanoparticles during Ultrasonic Cavitation Processing and Solidification of 6061-based Nanocomposites

D Zhang and L Nastac

The University of Alabama, Tuscaloosa, AL, 35487, USA

email: lnastac@eng.ua.edu

Abstract. The metal-matrix-nano-composites (MMNCs) in this study consist of a 6061 alloy matrix reinforced with 1.0 wt.% SiC 50 nm diameter nanoparticles that are dispersed uniformly within the matrix in large volume using an ultrasonic cavitation dispersion technique (UCDS) available in the Solidification Laboratory at UA. The required ultrasonic parameters to achieve the required cavitation for adequate degassing and refining of the aluminium alloy as well as the fluid flow characteristics for uniform dispersion of the nanoparticles into the 6061 matrix are being investigated in this study by using an in-house developed CFD ultrasonic cavitation model. The multiphase CFD model accounts for turbulent fluid flow, heat transfer and solidification as well as the complex interaction between the solidifying alloy and nanoparticles by using the Ansys's Fluent Dense Discrete Phase Model (DDPM) and a particle engulfment and pushing (PEP) model. The PEP model accounts for the Brownian motion. SEM analysis was performed on the as-cast MMNC coupons processed via UCDS and confirmed the distribution of the nanoparticles predicted by the current CFD model. A parametric study was performed using the validated CFD model. The study includes the effects of magnitude of the fluid flow and ultrasonic probe location (gravity direction).

1. Introduction

Aluminum-based metal matrix composites (MMCs) have been extensively studied and widely used in the aerospace, automotive and military industries due to their high strength-to-weight ratios and enhanced mechanical and thermal properties including specific modulus, superior strength, stiffness, good wear resistance, fatigue resistance and improved thermal stability [1-3]. However, the particles commonly used are micron-sized which has a counterpart that the ductility of the MMCs deteriorates with high ceramic particle concentration [4]. Consequently, more attention has been drawn to metal matrix nanocomposites (MMNCs), since the properties of metallic alloys reinforced by ceramic nanoparticles (with dimensions less than 100 nm) would be enhanced considerably while the ductility of the matrix is retained [5-11], because the incorporation of nano-sized reinforcements in metals and alloys will result in an Orowan-type strengthening mechanism where line defects are pinned by a uniform dispersion of particles within the grains, causing the dislocations to bow, and experimental evidence also shows that a significant degree of grain refinement (i.e., Hall-Petch strengthening) often occurs with additions of nanoparticles [12]. However, it is extremely difficult to obtain uniform dispersion of nano-sized ceramic particles in liquid metals due to high viscosity, poor wettability in the metal matrix, and a large surface-to-volume ratio, which results in agglomeration and clustering [4].

Currently, several fabrication technologies including high-energy ball milling [8, 11], in-situ synthesis [7], electroplating [13], and ultrasonic technology (UST) [4-5] are most commonly used, among which UST is supposed to be more reliable and cost effective.

During the solidification process, the particles will either be pushed or engulfed by the solidification front, among which particle pushing will always lead to segregation even clustering of the particulate reinforcement, which is undesirable as it results in non-homogeneous response and lower macroscopic mechanical properties. In general, it is considered that whether particles are pushed or engulfed during solidification depends on the velocity of the particle relative to the solidification front according to several previous models describing such particle engulfment and pushing phenomena [14-18]. However, these models only predict the behavior in the coarse (>> 1 μm) and fine particle (~ 1 μm) systems, and they don't accurately describe the ultrafine particle (<< 1 μm) system, presumably because the models rely on continuum mechanics. But these models cannot explain the evidence in MMNCs that nanoparticles can indeed be engulfed and distributed throughout the material and are not necessarily concentrated in grain boundary or interdendritic regions. As proposed by Ferguson [12], for sufficiently small particles, "Brownian Motion" can partially or completely counteract forces such as viscous drag, gravity and thermal/concentration gradients, thus leading to engulfment rather than pushing.

In this study, Ansys's Fluent Dense Discrete Phase Model (DDPM) [19] was adapted. The DDPM accounts for turbulent fluid flow, heat transfer, and the complex interaction between the molten alloy and nanoparticles during the melting and unidirectional solidification processes. Based on the theory proposed by Ferguson, all of the nanoparticles are assumed to be engulfed by the solidification front and no entrapment will occur. The dispersion of SiC nanoparticles with different injection positions, fluid flow intensities, and probe locations have been investigated in detail.

2. Model Description

The geometry of the model is shown in Figure 1. The ultrasonic probe has a diameter of 40 mm. The liquid aluminium alloy is 6061. It has a density of 2685 kg/m^3. The SiC nanoparticles with an average particle size of 55 nm and density of 3216 kg/m^3 are treated as inert-particles. The mass flow rate of the SiC nanoparticles is 0.014 kg/s. Thus, 1.0 wt.% of SiC nanoparticles can be injected at about 15 mm beneath the ultrasonic probe for 1 sec. The multiphase computational fluid dynamics (CFD) model accounts for turbulent fluid flow, heat transfer, and the complex interaction between the molten alloy and nanoparticles by using the ANSYS Fluent DDPM and k-ω turbulence model [19]. The CFD model is described in detail below.

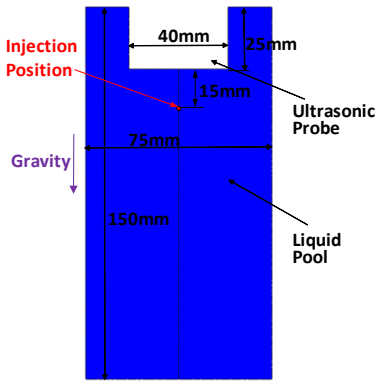

Figure 1. Geometry model

2.1. Fluid Flow Model

In the Eulerian DDPM multiphase model an Eulerian treatment is used for each phase, and the discrete phase (nanoparticles) is designated as a granular phase. The volume fraction of the particulate phase is accounted for in the conservation equations.
The continuity equation for the phase q is

$$\frac{\partial}{\partial t}\left(a_q \rho_q\right) + \nabla \cdot \left(a_q \rho_q \mathbf{u}_q\right) = \dot{m}_{pq} - \dot{m}_{qp} \tag{1}$$

The momentum balance for the phase *q* yields

$$\frac{\partial}{\partial t}\left(a_q\rho_q\mathbf{u}_q\right)+\nabla\cdot\left(a_q\rho_q\mathbf{u}_q\mathbf{u}_q\right)=-a_q\nabla P+\nabla\cdot\left[a_q\mu_q\left(\nabla\mathbf{u}_q+\nabla\mathbf{u}_q{}^T\right)\right]+a_q\rho_q g+\mathbf{f}_{DPM}+\mathbf{f}_{other} \quad (2)$$

where a_q is the phasic volume fraction, ρ_q is the density, $\mathbf{u}_q$ is the velocity, μ_q is the molecular viscosity, and P is the pressure shared by all phases. $\dot{m}_{pq}$ characterizes the mass transfer from the p^{th} to q^{th} phase, and $\dot{m}_{qp}$ characterizes the mass transfer from phase *q* to phase *p*. The momentum exchange term, $\mathbf{f}_{DPM}$, is considered only in the primary phase equations. The source term, $\mathbf{f}_{other}$, includes the virtual mass force, lift force, and turbulent dispersion force etc.
Equations (1) and (2) do not solve for the velocity field and volume fraction of the discrete phase. Their values are obtained from the Lagrangian tracking solution.

2.2. Solidification Model

The enthalpy method is used in the solidification model. The energy conservation equation of the enthalpy-formulation is

$$\rho\frac{\partial h}{\partial T}+\rho\nabla\cdot(\mathbf{u}h)=\nabla\cdot(k\nabla T)+Q_L \qquad \text{with} \qquad h=h_{ref}+\int_{T_{ref}}^{T}c_p dT \quad (3)$$

where *h* is the sensitive enthalpy, h_{ref} is the reference enthalpy at the reference temperature T_{ref}; c_p is specific heat; ρ and *k* are the density and thermal conductivity of the melting aluminium alloy, respectively, and $\mathbf{u}$ is velocity of the fluid.

The source term Q_L concerning the latent heat in a single phase solidification model can be written as

$$Q_L=\rho L\frac{\partial f_s}{\partial T} \quad (4)$$

where L is the latent heat and f_s is the solid fraction, which is assumed to vary linearly with the temperature in the mushy zone.

The mushy region is treated as a porous medium, and the porosity in each cell is set equal to the liquid fraction f_l in that cell. The momentum sink due to the reduced porosity in the mushy zone is:

$$\mathbf{S}=\frac{f_s^2}{(f_l^3+\varepsilon)}A_{mush}\mathbf{u} \quad (5)$$

where ε is a small number (0.001) to prevent division by zero; A_{mush} is the mushy zone constant, which measures the amplitude of the damping. The dynamic viscosity of the fluid also depends on the solid fraction which is related to temperature. It varies from 0.009 kg/(m·s) at the liquidus temperature to 1.0 kg/(m·s) below the coherency solid fraction (0.5).

2.3. Particle Tracking Model

The trajectory of a discrete phase particle is predicted by integrating the force balance on the particle. The force balance equates the particle inertia with the forces acting on the particle, and it is written as

$$\frac{d\mathbf{u}_p}{dt} = \mathbf{F}_D + \mathbf{F}_G + \mathbf{F}_B + \mathbf{F}_{virtual-mass} + \mathbf{F}_{pressure-gradient} + \mathbf{F}_{lift} + \mathbf{F}_{interaction} \quad (6)$$

where $\mathbf{u}_p$ is the particle velocity, and all the terms at the right-hand are with a unit of force/unit particle mass. The detailed description of the force terms shown in Equation (6) are presented in [19].

The chaotic effect of turbulence on the particle trajectories is accounted for using the stochastic tracking approach, i.e., the discrete random walk (DRW) model:

$$\mathbf{u} = \bar{\mathbf{u}} + \zeta\sqrt{2k/3} \quad (7)$$

where $\bar{\mathbf{u}}$ is the mean fluid velocity in the trajectory equation (9), ζ is a normally distributed random number, and k is the local turbulent kinetic energy.

Equation (6) can be cast into the following general form:

$$\frac{d\mathbf{u}_p}{dt} = \frac{1}{\tau_p}(\mathbf{u} - \mathbf{u}_p) + \mathbf{a} \quad (8)$$

where the term $\mathbf{a}$ includes accelerations due to other forces except drag force. Integrating the transport equation (8) for the path of each particle yields

$$\frac{d\mathbf{x}_p}{dt} = \mathbf{u} \quad (9)$$

where $\mathbf{x}_p$ is the particle position.

2.4. Boundary Conditions

The ultrasonic cavitation model is presented in Refs. [20, 21]. The ultrasonic cavitation model is uncoupled from the CFD nano-dispersion model because of significantly different time scales. The frequency used in the UST experiments is 18 kHz. However, modelling of ultrasonic cavitation takes place at a very small time scale (of the order of 10^{-5} to 10^{-7} s) and the fluid flow time scale is of the order of 10^{-2} to 10^{-3} s in this case. In order to account for the effects of ultrasonic stirring on the fluid flow-nanoparticle interaction, the ultrasonic probe surface is set as a velocity inlet sinusoidal profile with a frequency of 100 Hz (see Fig. 2), and therefore the time step in the nanodispersion simulations can be much higher (*i.e.*, 0.001s), which makes it possible to model the fluid flow with nanoparticles for much longer times with a reasonable computational time. After the initial transient, which is about 1s after adding the nanoparticles, and for the velocity profile shown in Fig. 2, the characteristics of the fluid flow and nanodispersion will remain unchanged. A similar trend was found at high frequencies.

All the walls are considered to be adiabatic before the solidification starts when the particles are well dispersed in the furnace. After that, the heat transfer boundary condition for the bottom wall of the furnace is set as constant temperature (500 °C) and all the other walls are still treated as adiabatic. All of the discrete phase boundaries are set as reflect. The interface between liquid 6061 alloy and air is pressure outlet and the other boundaries are set as wall.

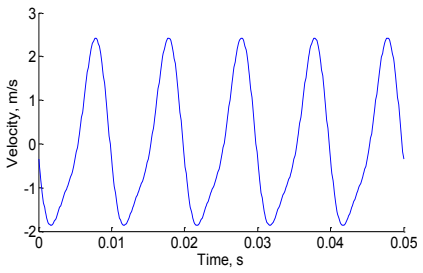

Figure 2. Velocity inlet profile

2.5. Solution Procedure

The SiC nanoparticles are injected at every fluid flow time step with a mass flow rate of 0.014 kg/s in the first sec. The distribution of the particle diameters varying from 45 nm to 65 nm follows the Rosin-Rammler expression. Particles are tracked at every time step after the fluid velocity field is solved. Because of the low volume fraction of the discrete phase, one-way coupling is employed, which neglects the effect of the discrete phase on the fluid turbulence.

3. Simulation Results and Discussion

Figure 3 shows the fluid flow and particle distributions after 1.0s, 3.0s, 10s and 30s, respectively. It can be seen that the flow is much stronger at the center of the furnace. It demonstrates that the particles have little effect on the fluid flow because of the one-way coupling, and the gravity direction is the same as the direction of the stronger flow in the center, so it will help to develop the fluid flow. Therefore the fluid flow after 3.0s is almost the same as that after 1.0s because both of them are fully developed (see Figs. 3(a) and 3(b)). The fluid flow is damped in the mushy zone, where the particles will move relatively slow and stop moving in the solid (see Figs. 3(c) and 3(d)). At 1.0s when the injection is stopped, newly injected particles are still at the center of the furnace where they are injected, since more time is needed for all of them to be dispersed into the liquid.

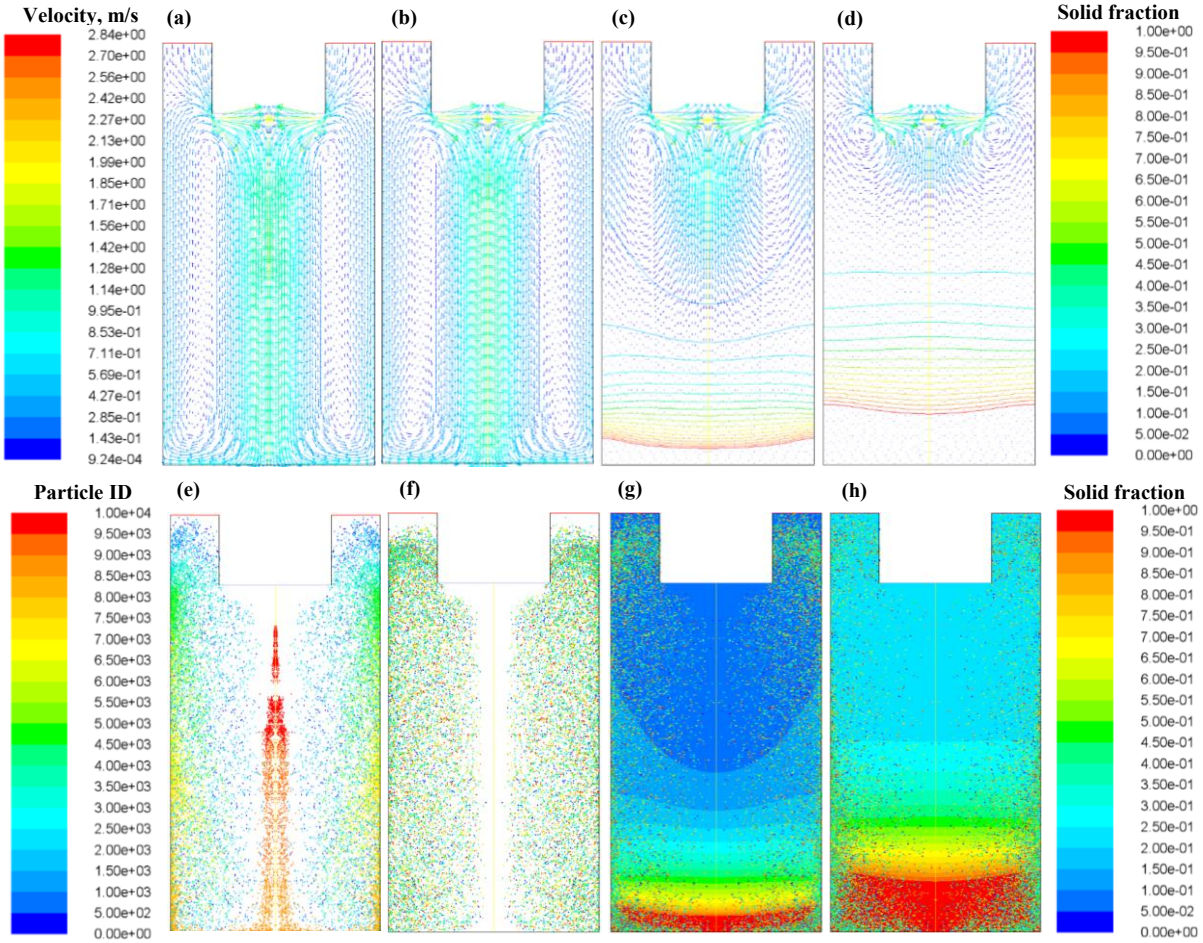

Figure 3. Fluid Flow and particle distributions (gravity direction downward, strong flow): (a) and (e) after 1.0s; (b) and (f) after 3.0s; (c) and (g) after 10s; and (d) and (h) after 30s.

Two seconds later, the particles have been dispersed pretty well from the bottom to the top, but a little more particles tend to stay near the wall, and fewer nanoparticles at the center where the flow is stronger, which indicates the nanoparticles couldn't disperse well in strong flows (see Fig. 3(f)). Additionally, the particle distribution stays almost the same henceforth which means the distribution becomes stable. Then, the solidification process starts at 3.0s, and in order to model the unidirectional solidification process, all the walls except the bottom one are treated as adiabatic. After 10s, we can see that there are some agglomerations in the solid (see Fig. 3(g)) because the nanoparticles approaching the solid/liquid interface will be engulfed based on the assumption that the Brownian motion will dominate during the particle engulfment/pushing process. It can be seen from Fig. 3(h) that after 30s the nanoparticles are dispersed quite well throughout the metal matrix, which is also validated by SEM analysis [22, 23]. To investigate the effect of the magnitude of the fluid flow on the nanodispersion, the velocity magnitude is changed to 1/10th of the original one shown in Fig. 2.

Figure 4 shows the fluid flow and particle distributions after 1.0s, 3.0s, 10s and 30s, respectively. As the fluid flow is weaker, the particle dispersion is slower. However, the flow pattern is similar as before (see Figs. 4(a) and 4(b)). But the flow fields after 1.0s and 3.0s are not exactly the same, because the flow after 1.0s is not fully developed. By the time when the injection is stopped (1.0s), most of the particles are at the top of the furnace where they are injected, because more time is needed to disperse them well in the liquid metal (see Fig. 4(e)).

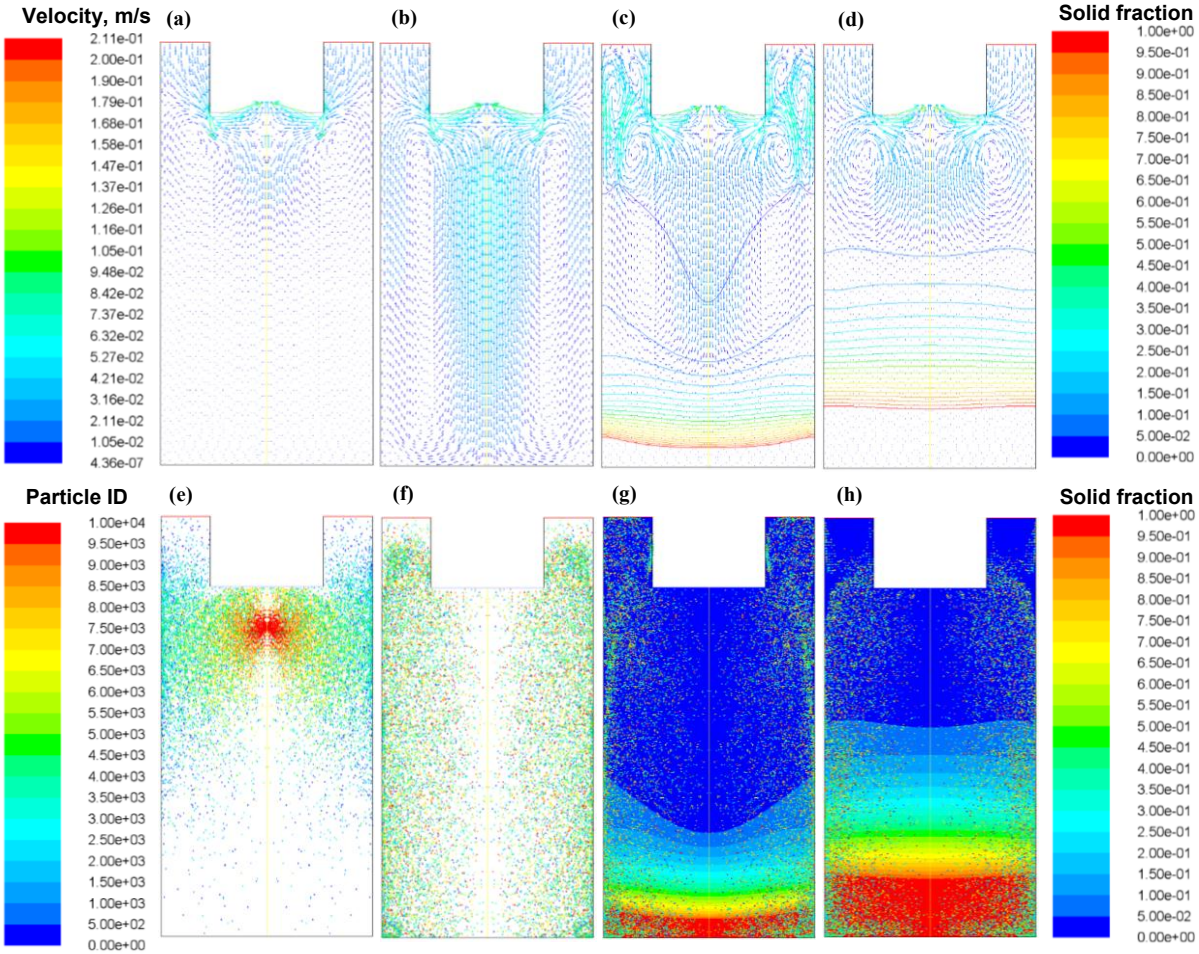

Figure 4. Fluid Flow and particle distributions (gravity direction downward, weak flow): (a) and (e) after 1.0s; (b) and (f) after 20s; (c) and (g) after 30s and (d) and (h) after 50s.

After 20s, the distribution of the nanoparticles becomes uniform and stable, and even more uniform than the case with a strong flow, because the difference between the fluid flow at the center of the furnace and that near the wall is not as significant as in the former case (strong flow). Then when the solidification starts 10s later, the overall distribution of the nanoparticles stays almost the same (see Fig. 4(g)). But after 50s, it is obvious that more particles are captured by the mushy zone, and almost no particles are at the top of the furnace, which indicates that the uniformity of the particles deteriorates (see Fig. 4(h)). Therefore, we can conclude that weak flow cannot disperse the nanoparticles well during the solidification process. To investigate the effect of the gravity direction, the ultrasonic probe is placed at the bottom of the furnace instead of the top as shown in Figure 5(a). Figure 5 presents the fluid flow and particle distributions after 1.0s, 3.0s, 10s and 20s, respectively.

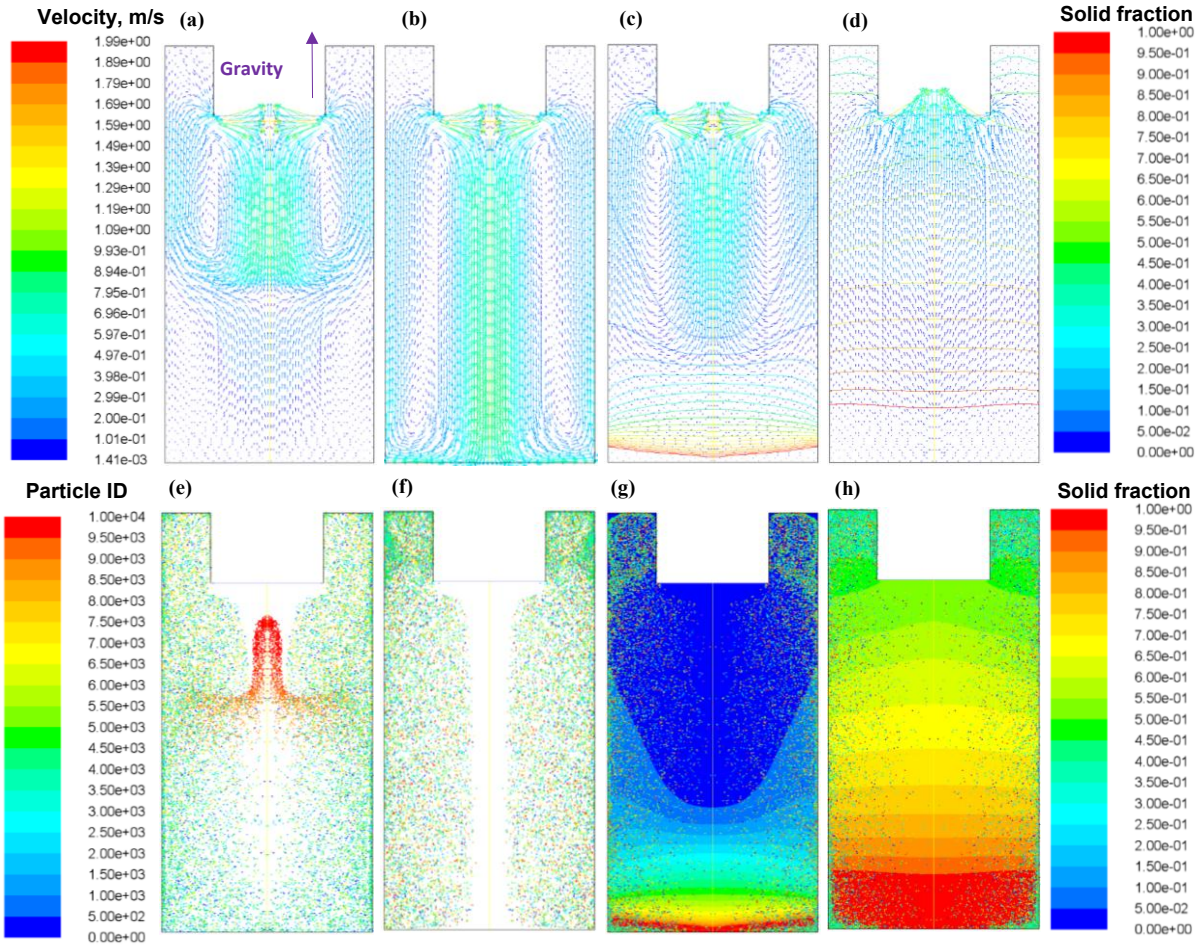

Figure 5. Fluid Flow and particle distributions (gravity direction upward, strong flow)): (a) and (e) after 1.0s; (b) and (f) after 3.0s; (c) and (g) after 10s and (d) and (h) after 20s.

It can be seen from Figs. 5(a) and 5(b) that the flow fields are not the same though a one-way coupling is used. This is because the gravity direction is opposite to the direction of the stronger flow in the center of the furnace, thus retarding the development of the fluid flow and resulting in a different flow pattern at 1.0s. But after 3.0s, the fluid flow is fully developed and becomes almost the same as that of the case with a different gravity direction, because the gravitational force is relatively weak compared to the drag force, if the flow is very strong. When the solidification starts after 3.0s, the fluid flow is damped in the mushy zone and becomes weaker, and then the gravity begins to play an import role in the flow. After 20s, the flow in the center even has an opposite direction as before, which is the same

as the gravity direction (see Fig. 5(d)), and accelerate the solidification process. As the solidification continues, the entire domain is fully solidified after only around 30s (this result is not shown in Fig. 5). The gravity effect on the dispersion of the nanoparticles is not significant in the fluid metal and the particle distribution is pretty uniform as before (see Fig. 5(f)). But as explained above, the gravity will make a big difference during the solidification process, reducing the solidification time and producing well dispersed nano-composites quickly.

4. Concluding Remarks and Future Work

The DDPM model coupled with the k-ω turbulence model is used to investigate the distribution of SiC nanoparticles into a 6061 matrix with different flow magnitudes and gravity directions under ultrasonic stirring and unidirectional solidification processing conditions. It was determined that a strong flow can disperse the nanoparticles relatively well, especially when compared with a weak flow condition. Also, it was demonstrated that the gravity direction can play a major role in the nano-dispersion during the solidification process. When the gravity direction is upward with respect with the location of the ultrasonic probe, the solidification time is decreased and thus well dispersed nano-composites can be produced faster than in the case when the gravity direction is reversed. The CFD nanodispersion model will be fully coupled with the ultrasonic cavitation model. The simulations will then be performed via a high performance computing cluster available at the University of Alabama.

References

[1] Kaczmar J W, Pietrzak K, Wlosinski W 2000 *J. Mater. Process. Technol.* **106** 58-67
[2] Durisinova K, Durisin J, and Orolinova M et al. 2012 *J. Alloys Compd.* **525** 137-142
[3] William C H 1998 *Mater. Sci. Eng., A* **244** 75–79.
[4] Yang Y, Lan J, Li X 2004 *Mater. Sci. Eng., A* **380** 378-383
[5] Cao G, Konishi H, Li X 2008 *Mater. Sci. Eng., A* **486** 357-362
[6] Shin J H, Choi H J, and Cho M K et al. 2014 *J. Compos. Mater.* **48** 99-106
[7] Dikici B, Gavgali M, Bedir 2010 *J. Compos. Mater.* **45** 895-900
[8] El-Daly A A, Abdelhameed M, and Hashish M et al. 2013 *Mater. Sci. Eng., A* **559** 384-393
[9] Jiang X, Galano M, Audebert F 2014 *Mater. Charact.* **88** 111-118
[10] Shin J H, Bae D H 2014 *Mater. Chem. Phys.***143** 1423-1430
[11] Borgohain C, Acharyya K, and Sarma S et al. 2013 *J. Mater. Sci.* **48** 162-171
[12] Ferguson J B, Schultz B F, and Rohatgi P K et al. 2014 *Light Metals TMS* 1383-1388.
[13] Sautter F K 1963 *J. Electrochem. Soc.* **110** 557
[14] Kim J K, Rohatgi P K 1998 *Metall. Mater. Trans. A* **29** 351-358
[15] Uhlmann D R, Chalmers B, and Jackson K A 1964 *J. Appl. Phys.* **35** 2986-2993
[16] Stefanescu D M, Moitra A, Kacar A S, and Dhindaw B K 1990 *Metall. Trans. A* **21** 231-239
[17] Shangguan D, Ahuja S, and Stefanescu D M 1992 *Metall. Trans. A* **23** 669-680
[18] Kaptay G 2001 *MetalL. Mater. Trans. A* **32** 993-1005
[19] Fluent 6.3: User's Guide Manual Fluent Inc. and Ansys's Fluent 2006 http://ansys.com/
[20] Nastac L 2011 *Metallur. and Mater. Trans.* B **42**(6) 1297-1305.
[21] Nastac L 2014 *Numerical Modeling of Fluid Flow and Solidification Characteristics of Ultrasonically Processed A356 Alloys. ISIJ Intern.* **54**(8) 1830-1835.
[22] Liu X, Jia S, Nastac L 2014 *Intern. Journal of Metal Casting (AFS)* **8** 1 1-12.
[23] Jia S, Allison P G, Rushing T W, Nastac L, Book Proceedings of *Advances in the Science and Engineering of Casting Solidification: An MPMD Symposium Honoring Doru Michael Stefanescu*, Eds. Nastac L *et al.*, TMS Conference, Orlando, FL, March 15-19, 2015 1-8.